ACS APPLIED MATERIALS & INTERFACES

Organic Electronic Devices

The Key Role of Side Chain Linkage in Structure Formation and Mixed Conduction of Ethylene Glycol Substituted Polythiophenes

Philip Schmode, Achilleas Savva, Robert Kahl, David Ohayon, Florian Meichsner, Oleksandr Dolynchuk, Thomas Thurn-Albrecht, Sahika Inal, and Mukundan Thelakkat

ACS Appl. Mater. Interfaces, **Just Accepted Manuscript** • DOI: 10.1021/acsami.9b21604 • Publication Date (Web): 18 Feb 2020

Just Accepted

is published by the American Chemical Society. 1155 Sixteenth Street N.W., Washington, DC 20036

The Key Role of Side Chain Linkage in Structure Formation and Mixed Conduction of Ethylene Glycol Substituted Polythiophenes

Philip Schmode [†], Achilleas Savva [‡], Robert Kahl [‖], David Ohayon [‡], Florian Meichsner [†], Oleksandr Dolynchuk [‖], Thomas Thurn-Albrecht [‖], Sahika Inal* [‡] and Mukundan Thelakkat* [†§]

[†]Applied Functional Polymers and §Bavarian Polymer Institute, University of Bayreuth, Universitätsstr. 30, 95440 Bayreuth, Germany

‡ Biological and Environmental Science and Engineering, King Abdullah University of Science and Technology (KAUST), Thuwal 23955-6900, Saudi Arabia

‖Experimental Polymer Physics Group, Martin Luther University Halle-Wittenberg, Von-Danckelmann-Platz 3, 06120 Halle, Germany

KEYWORDS: Bioelectronics, Organic Electrochemical Transistors, Polythiophenes, Mixed Conductors, Side-chain engineering

ABSTRACT: Functionalizing conjugated polymers with polar ethylene glycol side chains enables enhanced swelling and facilitates ion transport in addition to electronic transport in such systems. Here we investigate three polythiophene homopolymers (P3MEET, P3MEEMT and P3MEEET), having differently linked (without, methyl and ethyl spacer, respectively) diethylene glycol side chains. All the polymers were tested in organic electrochemical transistors (OECTs). They show drastic differences in the device performance. The highest μ_{OECT} C* product of 11.5 F/cmVs was obtained for ethyl spaced P3MEEET. How the injection and transport of ions is influenced by the side-chain linkage was studied with electrochemical impedance spectroscopy (EIS), which shows a dramatic increase in volumetric capacitance from 80± 9 up to 242±17 F/cm^3 on going from P3MEET to P3MEEET. Thus, ethyl-spaced P3MEEET exhibits one of the highest reported volumetric capacitance values among p-type polymers. Moreover, P3MEEET exhibits in dry thin films an OFET hole mobility of 0.005 cm^2/Vs, highest among the three, which is one order of magnitude higher than for P3MEEMT. The extracted hole mobility from OECT (oxidized swollen state) and the hole mobility in solid state thin films (OFET) show contradictory trends for P3MEEMT and P3MEEET. In order to understand exactly the properties in the hydrated and dry states, the crystal structure of the polymers was investigated with WAXS and GIWAXS and the water uptake under applied potential was monitored using E-QCMD. These measurements reveal an amorphous state for P3MEET and a semicrystalline state for P3MEEMT and P3MEEEET. On the other hand, E-QCMD confirms that P3MEEET swells ten times more than P3MEEMT in the oxidized state. Thus, the importance of the ethyl spacer towards crystallinity and mixed-conduction properties was clearly demonstrated, emphasizing the impact of side chain-linkage of diethylene glycol. This detailed study offers a better understanding how to design high performance organic mixed conductors.

1. INTRODUCTION

Side-chain engineering of conjugated polymers (semiconductors) is one of the most powerful strategies to modify the properties such as crystallinity, charge transport and solubility of conjugated polymers.[1] Especially polar side chains are of great interest in conjugated polymers, because they create a permanent dipole, decrease the dielectric constant, reduce the π- π stacking distance, enable enhanced swelling, facilitating simultaneous ionic and electronic transport (mixed conduction)[2–4]. In specific examples, it was also demonstrated that this modification improves the doping efficiency due to the higher miscibility of dopant molecules within the hydrophilic side chains.[5] In 2014, we demonstrated that conjugated polyelectrolytes (with ionic side chains) based on polythiophenes obtained using controlled polymerization are suitable candidates for mixed conduction.[6,7] However, due to their high solubility in water, device operation could only be realized after cross-linking the material. A strategy to reduce the amount of cross-linkers (which dilute the active semiconductor) is provided by copolymers of conjugated

polyelectrolytes and hydrophobic conjugated polymers.[8] Mixed conductors based on ethylene glycol (EG) substituted conjugated polymers are viable alternatives to conjugated polyelectrolytes. Their non-ionic hydrophilic EG side chains have been reported to facilitate ion transport and storage during biasing in aqueous electrolytes.[2,9] Thus, these polar conjugated polymers carrying EG side chains are potential candidates for biomedical and bioengineering applications and do not require any additional cross-linkers in aqueous media.[10] In general, the mixed conductors are attractive materials for several applications, such as thermoelectric devices, electrochromic displays and bioelectronics.[8,9,11,12]

The widely studied class of p-type semiconductors for bioelectronics still comprises of polythiophene derivatives, due to their high crystallinity, excellent charge carrier properties, high solubility and the feasibility of a controlled synthesis. The synthesis of substituted polythiophenes is of exceptional character, due to the quasi living polymerization character of the Kumada catalyst transfer polymerization, which was initially developed for poly-3-hexylthiophene (P3HT).[13–15] For bioelectronic applications, materials must show an excellent balance between a high ion transport and a high electronic charge transport, both of which are strongly correlated to the morphology of the polymers.[16,17] Both these properties are often contradictory, because ion conduction requires hydration, swelling and free volume of the polymer in aqueous medium, whereas high hole transport is generally observed in highly crystalline non-polar conjugated polymers.[18] For bioelectronic applications, organic electrochemical transistors (OECTs) provide a promising device configuration. In OECTs, small changes in ion fluxes in an electrolyte result in large changes in electrical output current, that is the channel current.[19] Here, the semiconductor material is in the channel which is in direct contact with the (typically aqueous) medium. During the operation of a p-type accumulation mode OECT, a small voltage applied at the gate electrode, V_G (< 1 V), injects anions into the channel compensating for the holes injected from the contacts, resulting in increased conductivity of the semiconductor.[19] Because of the change in the channel conductivity, the current between source and drain I_G increases.[18] The steady-state performance of OECTs can be expressed by their transconductance, g_m. The product μ_{OECT} C* of OECT mobility (μ_{OECT}) and volumetric capacitance (C*) was reported as figure of merit value, to benchmark the mixed conduction properties of materials and predict their performance in OECTs.[16] This product can be extracted from eq 1, using the measured transconductance g_m, V_{th} the threshold voltage, V_G the applied gate bias, and the geometry dependent OECT parameters such as the channel width (W) and channel length (L), as well as the channel thickness d.

$$g_m = \frac{\partial I_D}{\partial V_G} = \frac{W \cdot d}{L} \cdot \mu_{OECT} \cdot C^* \cdot (V_{th} - V_G) \quad (1)$$

The most studied polymer in OECTs is still poly(3,4-ethylenedioxythiophene) polystyrenesulfonate (PEDOT:PSS) due to its commercial availability, good mixed conductivity in doped state and high μ_{OECT} (1.9 cm^2V^{-1} s^{-1}) and moderate C* values (39 Fcm^{-3}).[16] PEDOT:PSS is available only in doped state and therefore the OECTs are operated in depletion mode. On the other hand, un-doped p-type conjugated copolymers equipped with EG sidechains and thienothiophene moieties working under accumulation mode have already reached μC* product values of around 300 $Fcm^{-1}V^{-1}$ s^{-1}. The best performing polymer of this class is poly(2-(3,3′-bis(2-(2-(2-methoxyethoxy)ethoxy)ethoxy)-[2,2′-bithiophen]5 yl)thieno [3,2-b]thiophene), p(g2T-TT).[20–22] In these materials, the ability of water molecules to form hydrogen bonds with EG allows swelling and facile ion penetration, necessary for electrochemical (i.e., bulk) doping. Also the fact that EG substituted polythiophenes are less soluble in water necessitates the use of external cross-linkers (also used in PEDOT:PSS) superfluous, which is advantageous for biolectronics.[23] Another example of polythiophenes functionalized with EG sidechains was reported by Flagg et. al.[24] They studied the influence of the size of the doping anion in OECTs using poly(3-{[2-(2-methoxyethoxy)ethoxy]methyl} thiophene-2,5-diyl) (P3MEEMT). They found that compared to P3HT, P3MEEMT has faster anion injection rates, which was attributed to the hydration of the P3MEEMT crystal lattice. However, the impact of the nature of the linkage of the ethylene glycol side chain on mixed conduction and OECT performance was not systematically studied up to now. The first report regarding the importance of the EG linkage came from another field, viz. Li^+-conduction for battery applications.[25] They investigated polythiophene derivatives with diethylene glycol side chains, where the first oxygen of the glycol side chain is directly connected to the thiophene core (P3MEET), or via a methyl spacer (P3MEEMT). They showed that the Li^+-ion conductivity (using added LiTFSI salt) increases in P3MEET.[25] But these polymers are neither studied for their mixed conduction properties nor compared in OECTs or OFETs.

Motivated by this observation of the large difference in Li^+-ion conduction, we wanted to investigate the influence of the nature of diethylene glycol linkage on mixed conduction, crystallinity and performance in OFET and OECT devices by systematical comparative studies. For this purpose, three ethylene glycol functionalized polythiophene derivatives were synthesized by controlled polymerization using KCTP. The diethylene glycol side

chains were linked either with no spacer (P3MEET), with a methyl spacer (P3MEEMT) or an ethyl spacer (P3MEEET). For a detailed comparative study of polymers prepared under same conditions, we synthesized the known polymers (P3MEET and P3MEEMT) and extended the series to a new polymer having ethyl spacer, P3MEEET. We elucidate the impact of EG side-chain linkage on the interplay of structure formation, swelling, volumetric capacitance and charge carrier mobility resulting in efficient mixed conduction properties. The three polymers differ in all the above properties drastically. For understanding these drastic differences in properties among the three polymers, we carried out first solid-state studies in thin films and bulk samples using OFET, XRD and AFM. These studies reveal that the crystallinity of P3MEEET reaches the highest value of 58 % in this series. Also, only P3MEEET showed a lamellar morphology in thin film. In line with these properties, P3MEEET with ethyl spacer linked EG side chain shows the best performance in OECT. From OECT measurements, the highest figure of merit value (μC* product) of 11.5 $Fcm^{-1}V^{-1}s^{-1}$ and highest volumetric capacitance of 242±17 F/cm^3 was determined for this ethyl-spacer polymer P3MEEET. To enable an explanation of the extraordinary OECT performance of P3MEEET, the ionic charge storage capability was quantified using electrochemical impedance spectroscopy. This study reveals a linear increase of the volumetric capacitance C* upon increasing the spacer length. E-QCMD measurements were carried out to evaluate the differences in water/ion uptake of the polymer films upon applying a doping potential in aqueous electrolyte. Out of these comprehensive and systematic studies, both in thin dry films and hydrated doped state of this series of three diethylene glycol functionalized polythiophenes, we could elucidate the unique properties associated with an ethyl spacer linkage of diethylene glycol in substituted polythiophenes.

2. EXPERIMENTAL SECTION

2.1. Materials. All chemicals were purchased from Sigma Aldrich or Fischer Scientific and used as received. P3HT was purchased from BASF SE (M_n = 15.6 kg/mol, Đ = 1.6, measured with SEC with THF as eluent and a polystyrene calibration). The detailed monomer and polymer synthesis are described in the Supporting Information.

2.2. Methods. 2.2.1**.** *^{1}H-NMR*. ^{1}H-NMR. Spectra were recorded in deuterated chloroform on a Bruker Avance 250 spectrometer at 300 MHz at room temperature. Chemical shifts are noted in ppm and coupling constants in Hz. All spectra were calibrated according to the residual solvent peaks ($CHCl_3$ δ=7.26 ppm).

2.2.2. Size exclusion chromatography (SEC). SEC was performed utilizing a Waters 515 HPLC pump and THF with 0.25 wt% tetrabutylammonium bromide (TBAB) as eluent at a flow rate of 0.5 mL/min. A volume of 100 μL of polymer solution (1-2 mg/mL) was injected with a 2707 Waters auto-sampler into a column setup comprising a guard column (Agilent PLgel Guard MIXED-C, 5 × 0.75 cm, particle size 5 μm) and two separation columns (Agilent PLgel MIXED-C, 30 × 0.75 cm, particle size 5 μm). Polymer size distributions were monitored with a Waters 998 photodiode array detector at 254 nm and a Waters 414 refractive index detector. Narrow distributed polystyrene standards were used for calibration and 1,2-dichlorobenzene as an internal reference.

2.2.3. Differential Scanning Calorimetry (DSC): A Perkin Elmer DSC 7 was used with a heating/cooling rate of 10 K/min. All samples 1st cooling and 2nd heating shown except for P3MEEMT: multiple measurements were conducted: max temperature increased gradually increased in steps of 10 °C from 80 to 130°C, two measurement runs each, measurement shown is 2nd measurement to 110°C.

2.2.3. Wide angle x-ray scattering (WAXS). Microfocus: A SAXSLAB laboratory Setup (Retro-F) (Copenhagen, Denmark) was used. As x-ray source, an AXO microfocus was used, with an AXO multilayer monochromator (Cu-K_α radiation λ=0.15418 nm, ASTIX) purchased from X-ray optics. For 2D Scattering patterns, a Dectris PILATUS R 300K detector (Daettwil, Switzerland) was used. SAXSGUI v2.19.02 was used for data reduction of the WAXS and SAXS patterns. All measurements were conducted under vacuo and WAXS in transmission, GIWAXS in reflection. Sample to Detector distance is around 89 mm. All samples measured in ordered temperature region and in melt, P3HT, P3MEEET during cooling run, P3MEEMT and P3MEET during heating run.

2.2.4. Spectroelectrochemistry Measurements. Thin films were prepared on ITO coated glass substrates. Measurements were carried out using a UV-Vis spectrometer (OceanOptics USB 2000+) integrated with an Ivium CompactStat potentiostat. A Pt mesh was used as the counter electrode and an Ag/AgCl electrode as the reference electrode. The indicated voltages were applied versus V_{OC} for 10 s until the current stabilized prior to recording of the spectrum**.**

2.2.5. Electrochemical Impedance Measurements (EIS). Electrochemical impedance spectroscopy (EIS) for determination of capacitance was measured on polymer coated electrodes with a Metrohm Autolab PGSTAT128N at a frequency range between 100 kHz to 0.1 Hz. The impedance spectra of the gate of the OECT (0.003364 cm^2 area) were measured in 0.1 M NaCl aqueous solution, using a standard Ag/AgCl as the reference electrode and a Pt mesh as the counter electrode. The measurements were performed at a DC offset potential which enables the maximum achievable doping for the material and an AC amplitude of 10 mV. Once the spectra were recorded, they were fit to equivalent circuit using native tool software Metrohm Autolab NOVA. For fitting, Randle's circuit was used, $R_{electrolyte}(R_{polymer}||C_{polymer})$, and resulted in good fit quality. The capacitance values that are extracted were normalized by the measured film volume to determine volumetric capacitance (C*). Thickness of films was measured in the dry state with a Bruker Dektac profilometer. See SI **Figure 10** for an example of experimental determination of volumetric capacitance.

2.2.6. Organic Field Effect Transistors (OFETs): Bottom gate/bottom contact organic field effect transistors (OFET Gen4) were purchased from Fraunhofer IPMS. N-doped silicon (doping at the surface n ~ 3 x 10^{17} cm^{-3}) was used as the surface and gate electrode. The dielectric consists of a 230 nm layer of silicon oxide. Each substrate consisted of 16 devices with a constant channel width of 10 mm and varying channel length of 2.5–20 μm. The source and drain electrodes were a 30 nm thick gold layer on a 10 nm ITO adhesion layer. The devices were prepared

by cleaning in acetone and subsequently in iso-propanol in an ultrasonic bath for 10 min, followed by 15 min treatment in an ozone oven at 50 °C and subsequent silanization by 45 min treatment in a bath of 1 wt% octadecyltrichlorosilane (ODTS) in toluene at 60 °C. The devices were rinsed with toluene and *i*-propanol and dried. Thin polymer films were spin cast from 5 mg/mL chloroform solutions at a spinning speed of 3000 rpm under ambient conditions. All devices were stored and measured under nitrogen atmosphere. The I-V-characteristics were measured using an Agilent B1500 semiconductor parameter analyzer. Using eq. (2) the charge carrier mobilities were calculated from the slope of the $(I^d)^{0.5}$– V_g plots.

$$I_d = \frac{W}{2L} C_i \mu \left(V_g - V_t\right)^2 \quad (2)$$

2.2.7. Atomic Force Microscopy (AFM). Measurements were performed on a Bruker MultiMode 8 AFM with a Nanoscope V controller equipped with a ScanAsystFluid+ cantilever (f_0 = 150 kHz, k = 0.7 Nm^{-1}) from Bruker. An excitation frequency of 2 kHz was used. Height and adhesion images (reflect strength of adhesive forces btw. Tip and surface) were recorded. Editing was done with open source software Gwyddion.

2.2.8. OECT Fabrication. The devices were fabricated according to the parylene-C lift-off method reported previously.[26] Standard glass microscope slides were cleaned via sonication in 2 % soap solution, acetone and isopropyl alcohol and dried with N_2. Connection pads and interconnects were deposited through a lift-off process using photolithographic patterning of two positive photoresists (LOR 5B and S1813). A subsequent metal deposition via sputtering of Cr (10 nm) and of Au (110 nm) and metal lift-off using NMP defines the Au lines. A first layer of parylene C (1.6 µm), deposited together with a small amount of 3-(trimethoxysilyl) propyl methacrylate (A-174 Silane) to enhance adhesion, acts as an insulator to prevent disturbing capacitive effects at the metal liquid interface. Subsequently, an antiadhesive layer was spin-coated using a dilution of industrial cleaner (2 wt %, Micro-90), and a second parylene-C sacrificial layer (2.1 µm) is deposited. To define the contact pads and the channel of the OECT, a second photolithographic patterning step using a thick positive photoresist (AZ9260) and AZ developer is used to protect the parylene-C layers from a subsequent plasma reactive ion etching step. All the polymer solutions were prepared in chloroform at 10 mg/mL and spin-coated from a glass fiber filter with 0.45 µm pore diameter. Peeling of the second parylene-C sacrificial layer defines the channel dimensions. The thickness of the channels was measured using a DEKTAK 150 stylus profilometer.

2.2.9. OECT Characterization. OECTs were characterized using a dual-channel source-meter unit (NI-PXI) with custom-written control code in LabVIEW. All measurements were performed using an Ag/AgCl pellet (D = 2 mm × H = 2 mm; Warner Instruments) as the gate electrode. The aqueous electrolytes were contained in a PDMS well on top of the OECTs, and the electrolyte volume was constant at 120 µL for all measurements.

2.2.10. E-QCM-D Swelling Experiments. Electrochemical Quartz crystal microbalance with dissipation monitoring: We performed EQCM-D measurements using a Q-sense analyzer (QE401, Biolin Scientific). Swelling measurements were performed as follows. First, we recorded the QCM-D response of the bare Au sensors in the air, followed by the injection of the $NaCl_{(aq.)}$ 0.1 M solutions into the chamber. This resulted in large shifts in frequency (f) and dissipation of energy (D), due to the density differences between the two media. The measurements were then stopped, the sensors were removed, and polymer films were spun cast directly on the same sensor from a 10 mg/mL chloroform solution at 1000 rpm. The absolute f value for each polymer coated sensor was obtained both in air and in $NaCl_{(aq.)}$ 0.1 M, after the f signal was perfectly flat (i.e., f <0.5 Hz) assuring that the system is in equilibrium. We then compared the absolute difference in f for multiple overtones between the bare sensor and the polymer coated sensors, both in air and in $NaCl_{(aq.)}$ 0.1 M by using the function "stitched data" of Q-soft software. This function compares the selected datasets based on the raw frequencies measured and excludes the effect of the different densities between the two media (**Figure S11**). Thus, the difference of the f values of the stitched data is directly analogous to the thickness of the polymer in both media, which is calculated by using the Sauerbrey equation below (**eq. 3**). EQCM-D measurements were performed using Autolab PGstat128N potentiostat coupled with Q-sense electrochemistry module. The three-electrode setup was comprised of Ag/AgCl reference, Pt counter and Au/polymer EQCM-D sensor as the working electrode. The physical modelling of the two measured parameters, the f and D, is related to the viscoelastic properties of the film. On the one hand, a rigid film shows zero D as there are theoretically no energy losses (no viscoelasticity) and Sauerbrey equation can be used to quantify the mass (m), using only one overtone as described in equation 3:

$$\Delta m = (-17.7)/n \, \Delta f_n \quad (3)$$

On the other hand, a thicker and/or softer film, does not follow the motion of the crystal and leads to energy losses during the oscillation. We approximate thicker and/or soft films to behave like a Kelvin-Voigt element, which means that they exhibit both viscous and elastic characteristics acting in parallel (viscoelastic). A Kelvin-Voigt element has a complex shear modulus as described in equation 4:

$$G^* = \mu + 2\pi i f \eta \quad (4)$$

where G^* is the complex shear modulus, µ is elasticity ($kgm^{-1}s^{-2}$), η is viscosity ($kgm^{-1}s^{-1}$) and f is the frequency. To calculate the mass changes of a thick, viscoelastic film, complex shear modulus was analysed and fitted using at least three frequency and dissipation of energy overtones. Q-Tools and D-find software were used for the modelling and data analysis. Since the polymer films are becoming soft and uptake a significant amount of water under doping potentials, we used the Kelvin-Voigt viscoelastic (VSE) model to fit the data. To quantify the mass correctly, we used the f and D data of three different overtones (3rd, 5th and 7th). The good quality of the fits guaranteed the accurate mass calculation accumulated within the films upon applied potentials.

3. RESULTS AND DISCUSSION

Three diethylene glycol functionalized thiophene monomers were synthesized, differing in the linkage of diethylene glycol side chain respective to the thiophene core in order to obtain the three polymers, P3MEET, P3MEEMT and P3MEEET (**Figure 1b**). The detailed monomers and polymer synthesis can be found in the supporting information (**Scheme S1**). For the polymer synthesis, we used the well-established Kumada Catalyst Transfer polymerization, with [1,3-

bis(diphenylphosphino)propane] dichloronickel (II) (Ni(dppp)Cl_2) as catalyst and tert-butyl magnesium chloride as Grignard metathesis reagent. All the polymerization reactions proceeded for four hours, which is noticeably longer than for 3-hexylthiophene monomer.[13] We assume that the catalyst Ni(dppp)Cl_2 probably coordinates to the ethylene glycol side chain (not only to the thiophene backbone), and so prolongs the polymerization.

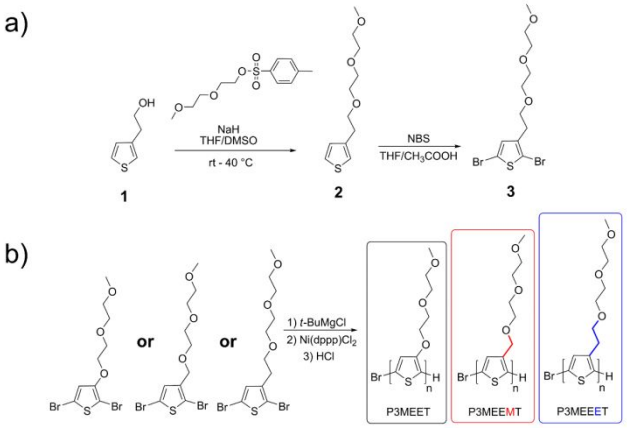

Figure 1: a) Newly developed synthetic route for the thiophene monomer 3MEEET (3) with an ethyl spacer. b) Kumada catalyst transfer polymerization procedure to obtain the polymers P3MEET (black), P3MEEMT (red) and P3MEEET (blue).

The polymers have narrow dispersity (Đ 1.08 to 1.4) and appreciably high molecular weight (~ 12 kg/mol) required for charge carrier transport, as determined with SEC measurements in THF. In the case of P3MEET, under our polymerization conditions in THF, we reached a maximum molecular weight of 10 kg/mol due to its limited solubility in THF and the relatively high reactivity of the monomer. The final polymers were purified using precipitation and Soxhlet extraction methods. P3MEEMT and P3MEEET are highly soluble in common solvents for polythiophenes, such as tetrahydrofuran and chloroform.

TGA studies reveal that the thermal stability of the polymers increases in the series from without spacer to ethyl spacer linkage of the EG unit. The lower thermal stability of P3MEET can be attributed mainly to the electron withdrawing effect of a directly connected EG unit (**Figure S1**). In differential scanning calorimetry experiments (DSC, **Figure S2**), a melting point for P3MEEET at 122 °C and a weak melting point for P3MEEMT at 99 °C can be observed, whereas P3MEET is an amorphous material. Both melting points as well as the melting enthalpies are noticeably lower compared to that of the benchmark polythiophene P3HT. These results indicate that EG side chains lead to reduced molecular order. The hole mobility in the dry state was extracted out of organic field effect transistors (OFETs). The hole mobility of the polymers was investigated in bottom-gate (Si) and bottom-contact (Au) devices with a silicon oxide layer as dielectric containing two different channels ranging from 10 to 20 µm. The polymer films were directly spin-coated from chloroform onto the substrates. By plotting the square root of the drain current I_D versus the gate voltage V_G the hole mobility can be estimated. The average value for the hole mobility was taken out of 4 transistor measurements. The output and transfer curves of the OFET measurements are depicted in **Figure S3**. Here, we observe a clear difference in the charge carrier mobility.

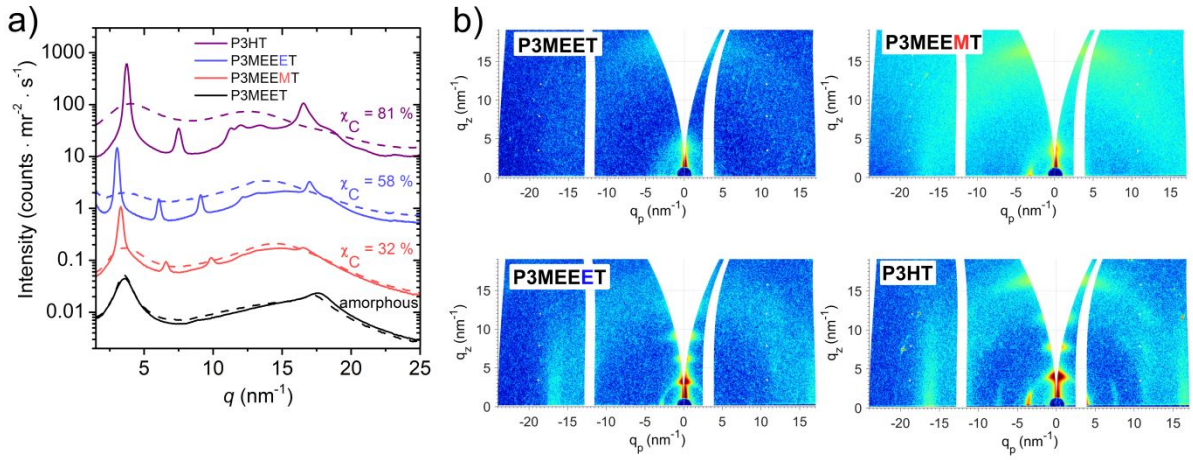

Figure 2: a) WAXS patterns of P3HT, P3MEEET, P3MEEMT and P3MEET. All samples were measured in ordered state (solid lines) and in the melt (dashed lines). b) Reciprocal space maps from GIWAXS of thin films of P3MEET, P3MEEMT, P3MEEET, and P3HT measured at an incident angle α_i = 0.20°. After spin coating, the polymer films except P3MEET were melt-crystalized in vacuo (P3HT, P3MEEET), respectively annealed (P3MEEMT at 70 °C).

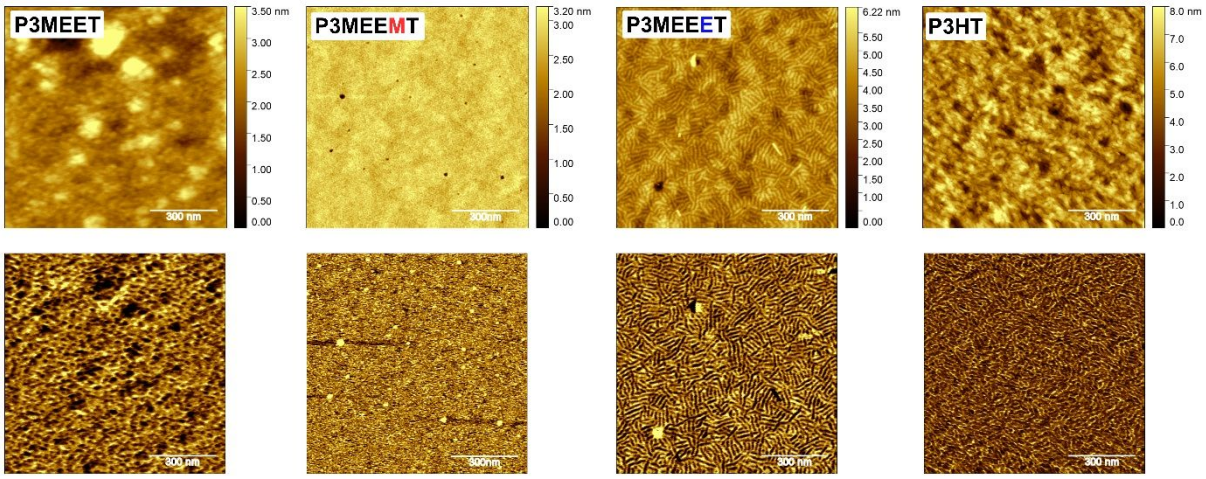

Figure 3: AFM pictures of P3MEET, P3MEEMT, P3MEEET, and P3HT recorded using peak force tapping mode. The height images are displayed in the upper row and the adhesion images are displayed in the lower row.

P3MEEET exhibits one order of magnitude higher hole mobility (0.005 cm^2/Vs) compared to P3MEEMT (0.0003 cm^2/Vs). With P3MEET, no transistor behavior could be observed. Compared to benchmark polythiophene P3HT, P3MEEET shows only one order of magnitude lower hole mobility and at the same time the highest reported value for a polar polythiophene homopolymer in transistors.[27]

To relate and possibly understand the differences in the hole mobility in the solid-state state of the different polymers in terms of microscopic structure, we performed X-ray scattering experiments in the bulk and in thin films. **Figure 2a** shows WAXS scattering pattern measured in transmission. All polymers except P3MEET were measured in the ordered state (solid line) and in the melt (dashed lines), whereby the exact temperature program for the different samples was adjusted according to their phase behavior observed in DSC (**Figure S2**). Generally, with decreasing length of the alkyl spacer between the first oxygen in the side chain and the polythiophene backbone, we observe a clear trend of decreasing order. This trend can be quantified in terms of the crystallinity, as estimated from the different intensities of the amorphous scattering contribution in between the first two Bragg-reflections according to Balko et. al.[28] For P3HT, the scattering pattern measured at 275 °C and at 20 °C after cooling from the melt is shown. The crystallinity amounts to 81 % comparable to values obtained in our previous studies.[28] For P3MEEET the measurement in the melt state was taken at 140 °C. While the crystal structure of P3MEEET is obviously similar to P3HT, the crystallinity shows a reduced value of 58%. For P3MEEMT the scattering pattern measured at 70 °C during a heating run is shown, as the sample does not recrystallize during cooling from the melt (150 °C), probably due to sample degradation. At this temperature the polymer is most well-ordered. In addition to a further reduced crystallinity of only 32 %, the (020) Bragg reflection is less pronounced. P3MEET finally shows only one much broader peak at the expected position of the (100) peak, which presumably corresponds to an amorphous structure. The measurement shown was taken at 20 °C as prepared and at 100°C. According to the earlier studies of P3HT crystal structure the lattice parameters of a monoclinic unit cell of P3HT were calculated from the WAXS peaks in Figure 2a (see Table 1).[28,29] Note that to determine the crystalline structure of the polymers precisely, a well oriented sample would be needed. As the GIWAXS patterns (Figure 2b) of both P3MEEMT and P3MEEET show only a few diffraction peaks, the crystal structure could not be determined from these measurements alone. However, the qualitative similarity between the WAXS of P3HT and P3MEEMT and P3MEEET suggests a similarity in their crystal structure. As such, we estimated the lattice parameters a and b for P3MEEMT and P3MEEET under the assumption of a monoclinic crystal lattice with the same angle γ as for P3HT (**Table 1**). While the b parameter does not show any significant change, the monotonic increase of the parameter a when going from P3HT to P3MEEET is expected, as the side chains become more voluminous.

Apart from molecular order or crystallinity, also molecular orientation can have a strong influence on transport properties. We therefore performed grazing incidence X-ray diffraction (GIWAXS, incident angle of α_i = 0.20°) experiments; the results are shown in **Figure 2b**). Complementary measurements taken at an incident angle α_i = 10° in order to access regions of higher q on the meridian gave consistent results and are shown in the Supporting Information (**Figure S4)**. The polymer films were spin coated onto Si-substrates and afterwards melt-crystallized in vacuo during slow cooling to room temperature. The film thicknesses used were approx. 20-30 nm. In all polymers, besides the amorphous P3MEET, the (100) peak is clearly visible with orientation perpendicular and parallel to the substrate, indicating a

mixed crystal orientation, but to different degrees. P3MEEET shows the strongest edge-on component. Overall, unlike the effects on crystallinity, we did not observe any strongly pronounced influence of the diethylene glycol linkage on the molecular orientation of ethylene glycol substituted polythiophenes on a Si substrate. Similar trends as in the scattering experiments could be observed in AFM images taken from the thin films samples used for GIWAXS.

Table 1: Crystal lattice parameters of P3HT, P3MEEMT and P3MEEET calculated from the corresponding WAXS patterns.

Polymer	a	b	c	γ
	(nm)	(nm)	(nm)	(°)
P3HT	1.677	0.757	0.788	92.7
P3MEEMT[a]	1.820	0.755	-	92.7[b]
P3MEEET	2.071	0.744	-	92.7[b]

a) Values calculated from WAXS measurement taken at 20°C to allow for comparison between materials. b) Values assumed based on similarity of scattering patterns to P3HT.

The AFM was operated in peak force tapping mode and **Figure 3** shows height and adhesion images. Consistent with the strong edge-on orientation of P3MEEET a very clear lamellar structure was observed for this sample. The morphology of P3HT appears somewhat weaker, as it is often found for commercial samples, but still well visible. For the other two samples P3MEEMT and P3MEET no clear structures can be discerned, consistent with the lower degree of order observed for these samples in the WAXS and GIWAXS data. Summarizing the results obtained from the structure analysis, the differences in the measured hole mobility in the investigated polymers can be explained neither by a change in the π-π-stacking distance nor by a change in the crystal orientation, which are known to have a strong influence on the charge carrier mobility.[30] Although further factors of influence cannot be ruled out, we suggest that the differences in the observed hole mobility are mainly caused by the differences in crystallinity.

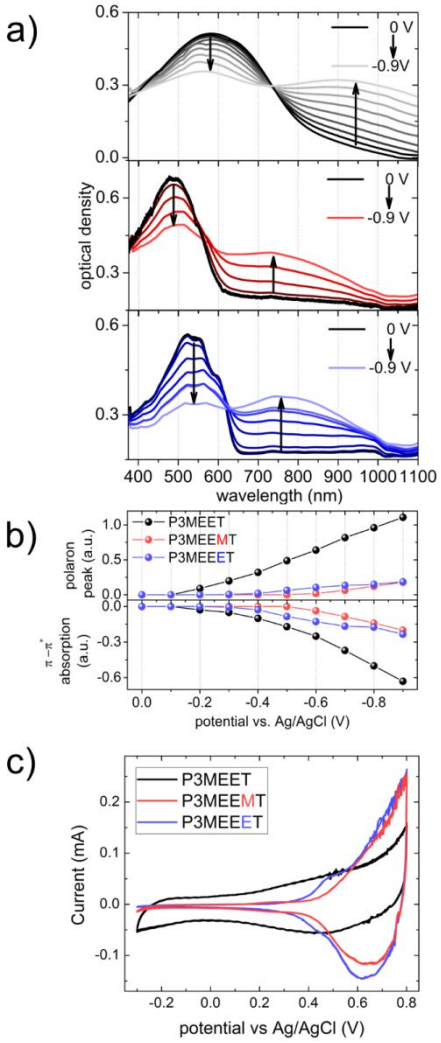

Figure 4: a) Spectroelectrochemistry measurements of polymer films on ITO of P3MEEET (blue), P3MEEMT (red) and P3MEET (black) respectively. The UV-Vis spectra were measured in 0.1 M NaCl when the films were biased from 0 V to - 0.9 V in a three-electrode setup with an Ag/AgCl reference electrode and a Pt counter electrode. b) Changes in the intensities of polaron peak (top) and π-π* absorption maximum (bottom), obtained from the difference spectra (Figure S6). c) Cyclic voltammetry (CV) measurements of the copolymer films were recorded with an Ag/AgCl reference electrode and a Pt counter electrode. CV curves were acquired at a scan rate of 50 mV s^{-1} in NaCl solution (0.1 M, aqueous).

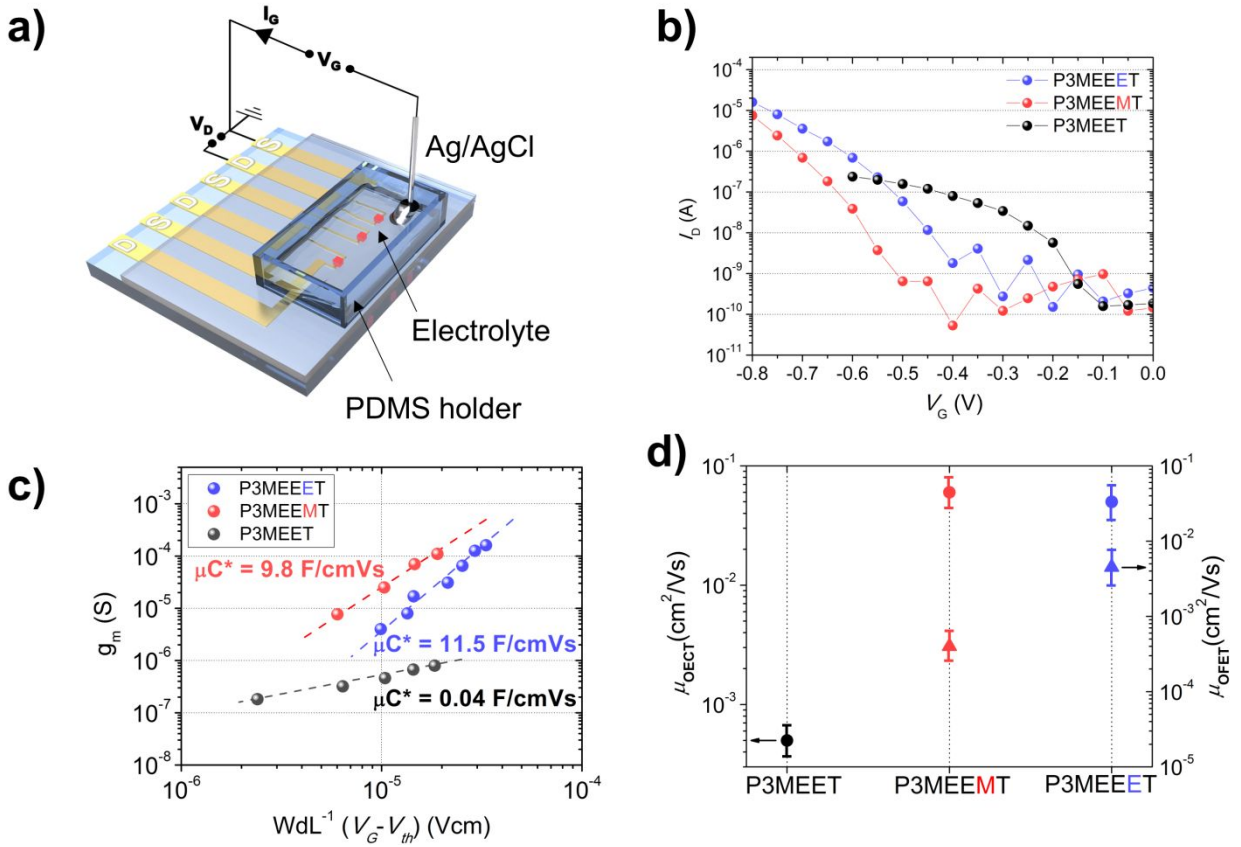

Figure 5: a) Illustration of an organic electrochemical transistor. The channel dimensions were *W*=100 µm and *L*=10 µm. OECTs were operated in 0.1 M aqueous NaCl solution with an Ag/AgCl pellet used as gate electrode. b) Transfer curve of P3MEET, P3MEEMT and P3MEEET. V_D = -0.6 V for P3MEET and V_D = -0.8 V for the other two polymers. c) Extracting the µC* product from the plot of transconductance g_m vs. the channel geometry and operation parameters. Dashed lines indicate the fits. d) OECT hole mobility extracted in the hydrated state plotted against the bulk hole mobility estimated from organic field effect transistors (OFETs, bottom-gate, bottom-contact geometry).

Our next questions are whether the polymers undergo oxidation at doping potentials applied in an aqueous medium and how the nature of the diethylene glycol side chain linkage affects the oxidation behavior of these polymers. This was investigated with spectroelectrochemistry (SEC) and cyclic voltammetry experiments in 0.1 M NaCl aqueous electrolyte. **Figure 4a** shows the UV-VIS spectra of the films subject to doping potentials (0 V to -0.9 V, in steps of -0.1 V, the neutral state is at 0 V, close to the open circuit potential, V_{OC}). In **Figure S5**, the relative changes in SEC spectra obtained by subtracting the pristine spectrum at 0 V (i.e., before application of voltage) from the spectrum of each oxidized state reached by varying doping potentials are shown. For all the three polymers, the main π-π* associated absorption intensity decreases and concomitantly a red-shifted polaron peak starts growing upon application of a doping potential. The evolution of the decreasing π-π* absorption maximum and the growing polaron peak is depicted in **Figure 4b**. The onset, as well as the oxidation of P3MEEMT and P3MEEET in aqueous solution is comparable, regarding the extent of oxidation. The intensity of the polaron peak of P3MEET is substantially higher than that of the polymers with spacers when biased at the same doping voltages. Moreover, the onset of the oxidation for P3MEET is very low at around -0.2 V, whereas the polymers containing methyl and ethyl spacers exhibit higher onsets of about -0.5 to –0.6 V. Both observations can be explained as due to the ease of oxidation of P3MEET, which in turn can be attributed to its low ionization potential. This agrees very well with the photon electron spectroscopy in air (PESA) results discussed later. Furthermore, we recorded cyclic voltammetry (CV) curves of the polymer films in 0.1 M NaCl solution (**Figure 4c**). As expected from PESA and SEC studies, a drastic difference on the oxidation onset is observed; P3MEET showing an early onset at 0.1V. P3MEEMT and P3MEEET on the other hand show pronounced oxidation in contact with the electrolyte, with oxidation onset for P3MEEMT at around 0.5 V and for P3MEEET at around 0.4 V, which also corresponds to the threshold voltage V_{th} observed in OECT operation as discussed below.

Since all polymers exhibit oxidation behavior in aqueous environment at low applied voltages (<0.7 V vs Ag/AgCl), the next step is to test them in OECT devices in order to quantify the mixed conduction properties. **Figure 5a** illustrates the OECT geometry which was used to examine the mixed conduction properties of the three functionalized polythiophenes. The fabrication of the devices is described in the supporting information.[31] **Figure 5b** depicts the transfer curves of OECTs comprising these three polymers operated in 0.1 M NaCl solution (see the output curves and additional transfer curves in **Figure S7, S8 and S9**).

Table 2: Summary of the polymer properties: molecular weight, polydispersity, thermal properties and the mixed conduction properties volumetric capacitance C*, the normalized transconductance g_m and the material dependent μ_{OECT} C* product.

Polymer	M_n (Đ)[a]	T_m[b]	ΔH_m[b]	Volumetric Capacitance C*[c]	Threshold Voltage V_{th}[d]	I_P[e]	Transconductance g_m[f]	Figure of Merit μ_{OECT} C*[g]
	(kg/mol)	(°C)	(J/g)	(F/cm^3)	(V)	(eV)	(S/cm)	(F/cmVs)
P3MEET	10 (1.43)	-	-	80±9	-0.18	-4.50	0.02	0.04±0.01
P3MEEMT	12 (1.21)	99	2.0	160±12	-0.66	-4.70	12.3	9.8±1.1
P3MEEET	13 (1.08)	122	8.6	242±17	-0.57	-4.66	20.4	11.5±1.4

a) SEC, with THF as eluent and against polystyrene standards. b) DSC in nitrogen atmosphere and a heating rate of 10 K/min. c) Electrical impedance spectroscopy (EIS) on Au electrodes with a DC voltage of 0.6 V (for P3MEET) or 0.8 V vs Ag/AgCl (for P3MEEMT and P3MEEET). d) V_{th} was determined from Figure S7 by extrapolating the linear region of the curve. e) Ionization potentials were estimated with PESA experiments (Figure S9) f) g_m at V_G = -0.6 V and V_D = -0.8 V and normalized by the film thickness. g) The μ_{OECT} C* product was extracted from Figure 5c.

We measured comparable thicknesses for the polymer films, between 90 and 100 nm, patterned on microscale Au patterns adjacent to the channels. Amongst all OECTs, the maximum drain current I_D was observed for the ethyl spacer derivative, P3MEEET, whereas the maximum transconductance (at a gate voltage V_G = -0.8 V) was measured for P3MEEMT and P3MEEET. The OECT characteristics are summarized in **Table 2**. Notably, P3MEET in which the diethylene glycol side chain is directly connected to the thiophene backbone exhibits a very low threshold voltage V_{th} of -0.18 V, compared to the polymers with a methyl and an ethyl spacer. This can be mainly attributed to the increased electron withdrawing effect of the directly connected oxygen in P3MEET making this polymer easily oxidizable. To understand the differences in the threshold voltages, the ionization energies (I_P) were measured using photon electron spectroscopy measurements in air (PESA, **Figure S9**). These measurements reveal that the I_P value is the lowest for P3MEET (I_P =-4.5 eV) compared to the other two polymers with methyl or ethyl spacers, which explains the observed low threshold voltage in OECT operation for the former. This is also in agreement with the SEC and CV results discussed above. In comparison with the Ip value of P3HT (-4.67 eV)[32], P3MEEMT and P3MEEET show similar values. This can be possibly explained by the methyl and ethyl spacer in the latter which makes them similar to P3HT. The easiness of oxidation in P3MEET originates from the direct oxygen connection without any spacer.´´.

In order to determine the μ_{OECT} C* product, **eq 1** was used. By plotting the transconductance g_m against the channel geometry and operation parameters of the OECT, μ_{OECT} C* can be estimated from the slope of the curve fit to the linear regime (**Figure 5c**). In aqueous 0.1 M NaCl solution, the μ_{OECT} C* product for P3MEEMT (9.8 F/cmVs) and P3MEEET (11.5 F/cmVs) are similar and considerably higher than that for P3MEET (0.04 F/cmVs). Thus, P3MEEET with ethyl-spacer is the most promising candidate for bioelectronic applications. It is also to be noted that all these polymers were tested in OECTs without the need of any cross-linker. It is known that OECT characteristics depend also on the nature of the electrolyte.[20] An electrolyte containing divalent anions or anions with different polarity may result in an increased capacitance and/or increased charge carrier mobility of the semiconductor, which can be applied in the case of P3MEEET to further improve the performance of the OECTs made thereof.

To investigate the charge storage capability, measurements of electrochemical impedance spectroscopy (**Figure S10**) of the polymers were recorded for the film before doping (V = V_{OC}) and at a doping potential that gives the maximum transconductance (V= -0.8 V for P3MEEMT and P3MEEET and -0.6 V for P3MEET vs Ag/AgCl). The impedance data were fit to Randle´s circuit $R_{electrolyte}(R_{polymer}||C_{polymer})$ to extract the capacitance of the polymers, which was then normalized by the volume of the films to estimate the volumetric capacitance C*. The volumetric capacitance increases from

80±9 to 160±12 and 242±17 F/cm^3 when going from P3MEET without a spacer to P3MEEMT and P3MEEET having a methyl or an ethyl spacer. The volumetric capacitance of P3MEEET is in the range of the highest reported value for the benchmark-type mixed conductor polymer p(g2T-TT).[16] The electrochemical charging in undoped (p-type) conjugated polymers involves simultaneous anion injection from the electrolyte and hole injection from the metal electrodes. Thus, a capacitor is formed between these two carriers, which is the origin of the capacitance of the polymer film. Proctor et. al. described that the volumetric capacitance C* can be directly associated with the density of these anion/hole pairs in the polymer.[33] We attribute the increase in C* to better accessibility of the mobile holes to the penetrating anions. Sivaraman et. al. linked the increased capacitance of P3HT with a higher crystallinity and order.[34] They attributed an increase in capacitance in higher crystalline P3HT derivatives to a decreased resistance for ion motion in the film. Furthermore, they observed that the highly disordered amorphous phase poses more restriction to the drift of ions. Thus, an increased volumetric capacitance C* in P3MEEET, compared to P3MEEMT and P3MEET can be explained by the higher crystalline order and their regioregularity. Additionally, the high capacitance of P3MEEET can be well-understood if the swelling and water/ion uptake of this polymer is considered as discussed later. Based on the capacitance values and the μ_{OECT} C* product extracted from OECT measurements, the hole mobility μ_{OECT} of the three polythiophenes can be estimated. μ_{OECT} describes the mobility in the swollen oxidized state under OECT operation and therefore strongly depends on the structural order of the polymer in the swollen and oxidized state, as well as the used electrolyte. High hole mobility in polythiophenes is generally observed in well-ordered systems, thus a large swelling in OECT operation can lower the effective hole mobility of the system, if the morphology or crystallinity in electrolyte medium is unfavorable for charge hopping.[21].

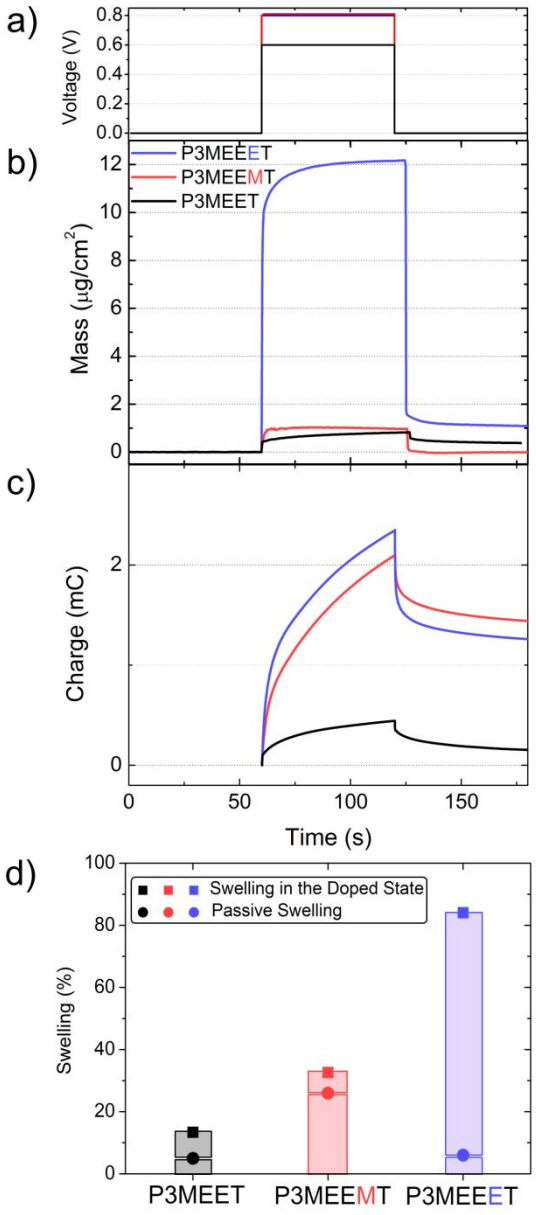

Figure 6: a) Doping potential profile applied to the polymer films, 0.8 V for P3MEEMT and P3MEEET and 0.6 V for P3MEET vs Ag/AgCl. b) mass change and c) the corresponding charge recorded as the polymers were doped. All measurements were performed in NaCl 0.1 M with an Ag/AgCl reference and Pt counter electrode, and the polymer film was deposited on QCM-D crystal with an area of 0.7854 cm2. d) The swelling percentage of polymer films as they were exposed to the electrolyte and upon the application of the doping potential.

From OECT measurements, similar hole mobilities were obtained for P3MEEMT and P3MEEET (0.06 cm^2/Vs and 0.05 cm^2/Vs), whereas P3MEET exhibits a lower mobility in the swollen state (5.2 ·10^{-4} cm^2/Vs). Comparing the μ_{OECT} values (measured in hydrated state) to the μ_{OFET} values obtained in thin dry films allows us to draw conclusions regarding the change in structure or morphology due to

swelling (**Figure 5d**). It is very interesting to note that P3MEET is clearly an OECT material although it did not show any transistor characteristics in OFET configuration, indicating that swelling might have a positive influence on the charge transport for this polymer. On the other hand, P3MEEET (with the highest crystallinity in solid state), which showed one order of magnitude higher OFET mobility compared to P3MEEMT, forfeit this advantage in swollen state in OECT devices. These results can be understood only if the swelling behavior of the three polymers are studied under applied voltages. In order to understand the influence of EG linkage on swelling and water/ion uptake properties of these conjugated polymers, we used electrochemical quartz crystal microbalance with dissipation monitoring (EQCM-D).[35–37] EQCM-D allows monitoring of mass exchange between an electrically active film and an electrolyte as the film undergoes electrochemical doping/de-doping. Here we study, simultaneously, the mass (ions and water) taken-up by the polymer films and the amount of charge generated during the electrochemical doping. First, we measure the passive swelling of the three polymers cast on QCM-D sensors as they are exposed to 0.1 M NaCl solution. The passive swelling percentage was calculated using Sauerbrey model (**Eq. 3**).[23,35] The pristine films swell 5 % ± 2 % (P3MEET), 26 % ± 8 % (P3MEEMT) and 6 % ± 3 % (P3MEEET) of their initial mass when exposed to the electrolyte (**Figure S11**). Here we observe that degree of passive swelling follows the order; P3MEEMT (methyl spacer) > P3MEEET (ethyl spacer) > P3MEET. The trend in passive swelling could not be correlated with the swelling in doped state and hence we avoided speculations to explain this trend. We assume that it may be linked to the morphology of the polymers in thin film prior to swelling. However, in the AFM images shown in our manuscript, we do not observe any structural features for P3MEEMT, whereas in P3MEEET shows a strong lamellar order, which could inhibit water absorption.

This order completely changes when measuring the amount of mass uptake triggered by a doping potential. The voltage pulses used for each polymer film are also the voltages that enabled the maximum transconductance. Upon application of a doping potential to the films (with a magnitude that corresponds to the maximum transconductance in OECTs), we monitor tremendous differences in the water and ion uptake (**Figure 6b** and **d**). Due to the large changes in the dissipation, we used a Kelvin-Voigt viscoelastic model to interpret the swelling behavior and to calculate the mass uptake.[38] P3MEEET takes up noticeably more mass compared to P3MEEMT and P3MEET. The total mass (water and Cl^- ions) accumulating inside P3MEEET during oxidation is about 12 µg/cm^2, whereas P3MEET and P3MEEMT take up around 1.0 µg/cm^2 (see **Figure S12** for the recorded raw frequency and dissipation changes). This 12 times higher mass uptake of P3MEEET during the penetration of electrolyte anions is by far the highest value reported up to date, compared to other mixed conductors, as well as the benchmark accumulation mode material p(g2T-TT) when it is doped to approximately to the same oxidized state.[20,21] Furthermore, the charge recorded from these films in-situ upon electrochemical doping with Cl^- ions is calculated to be $2.33 \cdot 10^{-3}$ C for the P3MEEET film and $2.1 \cdot 10^{-3}$ C for the P3MEEMT film, while it is $4.4 \cdot 10^{-4}$ C for P3MEET, which were then normalized by the film thickness, resulting in 45.4 C/cm for P3MEET, 135.5 C/cm for P3MEEMT and 153.3 C/cm for P3MEEET. These values are well in line with the volumetric capacitance calculated from the electrochemical impedance spectra of films recorded in OECT channels (**Figure S10**) and demonstrate the improvement in the ionic charging of the ethylene glycol functionalized polythiophenes as a result of side-chain engineering. Why exactly an ethyl-spacer linked diethylene glycol (in P3MEEET) causes this strong ability of water and ion uptake in the oxidized state compared to no spacer or methyl spacer is not yet fully understood. Additionally, it seems that the μ_{OECT} values also correlate with the charging in the hydrated system. The observed swelling in E-QCMD measurements for P3MEET (with no measurable μ_{OFET} mobility) resulting in measurable μ_{OECT} also supports this assumption. However, we like to point out that mixed conduction in differently swollen and differently oxidized systems is very complex and difficult to be correlated with the individual material properties in solid state, for example the charge carrier mobilities in thin dry films.

4. CONCLUSION

A detailed study of the impact and importance of the nature of linkage of diethylene glycol side chain functionalized polythiophene derivatives towards the mixed conduction and solid-state properties was presented. Three defined polythiophenes equipped with diethylene glycol side chains (P3MEET, P3MEEMT and P3MEEET), varying the side-chain linkage respective to the thiophene backbone (without, methyl and ethyl spacer), were synthesized in a controlled manner with similar molecular weights and low polydispersity. The suitability of these polymers for OECT applications was tested using SEC, UV-Vis and CV measurements performed in an aqueous medium. We found that the low oxidation onset observed for P3MEET correlates with the low ionization energy measured with PESA. The solid-state hole mobility of the polymers was determined using OFET configuration. Here, P3MEEET exhibits the highest reported value (0.005 cm^2/Vs) for a polar polythiophene homopolymer and this is one order of magnitude higher compared to the polymer with methyl spacer (P3MEEMT).

This increase in the solid-state hole mobility can be attributed to the higher crystallinity of P3MEEET compared to P3MEEMT as revealed by the WAXS. The differences in molecular order were also confirmed by AFM, where only P3MEEET shows a lamellar morphology. A possible application in bioelectronic devices was tested with organic electrochemical transistors in 0.1 M NaCl. Drastic differences in the performance of the three conjugated polymers could be observed, where P3MEEET (ethyl spacer) shows the best mixed conduction properties with a μ_{OECT} C* product of 11.5 (F/cmVs). To understand the influence of linkage of diethylene glycol side chain and the extraordinary performance of P3MEEET, the ionic charge storage capability was tested using electrochemical impedance spectroscopy. This study reveals a linear increase of the volumetric capacitance C* upon increasing the spacer length. This can be presumably attributed to a better accessibility of the diethylene glycol side chain and thus an enhanced ion transport, as well as a higher order of P3MEEET. P3MEEET exhibits a volumetric capacitance of around 242±17 F/cm^3, which is in the range of the highest reported values for p-type organic mixed conductors.[16] From OECT device characteristics, the hole mobility (μ_{OECT}) of the polymers in the hydrated state was extracted. The μ_{OECT} of the P3MEEMT and P3MEEET are almost identical in the swollen state. The differences in water uptake and swelling were monitored with E-QCM-D experiments, without (passive swelling) and under applied doping potential. P3MEEET takes up 12 times more water and ions than P3MEET and P3MEEMT in the oxidized state. The charge uptake derived from the same measurements correlate well with the volumetric capacitance. Thus, the nature of linkage, which may seem to be trivial plays an enormously important role in deciding the complex interplay of swelling, ion uptake and charge transport in OECTs. We conclude that this systematic and comparative study combining various interdisciplinary characterization techniques gives insights into determining factors influencing mixed conduction. Overall, this contribution emphasizes the crucial role of side-chain engineering in diethylene glycol substituted polythiophenes towards high performance polymeric mixed conductors.

ASSOCIATED CONTENT

Supporting Information

Detailed monomer and polymer synthesis, Thermal characterization (TGA, DSC), OFET transfer and output curves, GIWAXS at an incident angle of α = 10°, SEC difference spectra, Additional OECT characterization, PESA measurements, Impedance, QCM-D and EQCM-D raw frequency and dissipation changes at different overtones.

AUTHOR INFORMATION

Corresponding Author

*E-mail: mukundan.thelakkat@uni-bayreuth.de
*E-mail: sahika.inal@kaust.edu.sa

ACKNOWLEDGMENT

We acknowledge financial support from DFG (GRK 1640) and Bavarian State Ministry for Education, Science and the Arts (Project: SolTech). Additional funding by the European Union (EFRE) is gratefully acknowledged.

REFERENCES

(1) Mei, J.; Bao, Z. Side Chain Engineering in Solution-Processable Conjugated Polymers. *Chemistry of Materials* **2014**, *26* (1), 604–615.

(2) Giovannitti, A.; Maria, I. P.; Hanifi, D.; Donahue, M. J.; Bryant, D.; Barth, K. J.; Makdah, B. E.; Savva, A.; Moia, D.; Zetek, M.; Barnes, P. R. F.; Reid, O. G.; Inal, S.; Rumbles, G.; Malliaras, G. G.; Nelson, J; Rivnay, J.; McCulloch, I. The Role of the Side Chain on the Performance of N-Type Conjugated Polymers in Aqueous Electrolytes. *Chemistry of Materials* **2018**, *30* (9), 2945–2953.

(3) Liu, J.; Qiu, L.; Alessandri, R.; Qiu, X.; Portale, G.; Dong, J.; Talsma, W.; Ye, G.; Sengrian, A. A.; Souza, P. C. T.; Loi, M. A.; Chiechi, R. C.; Marrink, S. J.; Hummelen, J. C.; Koster, L. J. A. Enhancing Molecular N-Type Doping of Donor-Acceptor Copolymers by Tailoring Side Chains. *Adv. Mater.* **2018**, *30* (7), 1704630.

(4) Meng, B.; Song, H.; Chen, X.; Xie, Z.; Liu, J.; Wang, L. Replacing Alkyl with Oligo(Ethylene Glycol) as Side Chains of Conjugated Polymers for Close π–π Stacking. *Macromolecules* **2015**, *48* (13), 4357–4363.

(5) Kiefer, D.; Giovannitti, A.; Sun, H.; Biskup, T.; Hofmann, A.; Koopmans, M.; Cendra, C.; Weber, S.; Anton Koster, L. J.; Olsson, E.; Rivnay, J.; Fabiano, S.; McCulloch, I.; Müller, C. Enhanced N-Doping Efficiency of a Naphthalenediimide-Based Copolymer through Polar Side Chains for Organic Thermoelectrics. *ACS Energy Lett.* **2018**, *3* (2), 278–285.

(6) Brendel, J. C.; Schmidt, M. M.; Hagen, G.; Moos, R.; Thelakkat, M. Controlled Synthesis of Water-Soluble Conjugated Polyelectrolytes Leading to Excellent Hole Transport Mobility. *Chemistry of Materials* **2014**, *26* (6), 1992–1998.

(7) Schmidt, M. M.; ElMahmoudy, M.; Malliaras, G. G.; Inal, S.; Thelakkat, M. Smaller Counter Cation for Higher Transconductance in Anionic Conjugated Polyelectrolytes. *Macromolecular Chemistry and Physics* **2018**, *219* (2), 1700374.

(8) Schmode, P.; Ohayon, D.; Reichstein, P. M.; Savva, A.; Inal, S.; Thelakkat, M. High Performance Organic Electrochemical Transistors Based on Conjugated Polyelectrolyte Copolymers. *Chem. Mater.* **2019**, *31* (14), 5286–5295.

(9) Inal, S.; Rivnay, J.; Suiu, A.-O.; Malliaras, G. G.; McCulloch, I. Conjugated Polymers in Bioelectronics. *Accounts of Chemical Research* **2018**, *51* (6), 1368–1376.

(10) Zhao, H.; Zhu, B.; Sekine, J.; Luo, S.-C.; Yu, H. Oligoethylene-Glycol-Functionalized Polyoxythiophenes for Cell Engineering: Syntheses,

Characterizations, and Cell Compatibilities. *ACS Applied Materials & Interfaces* **2012**, *4* (2), 680–686.

(11) Collier, G. S.; Pelse, I.; Reynolds, J. R. Aqueous Electrolyte Compatible Electrochromic Polymers Processed from an Environmentally Sustainable Solvent. *ACS Macro Lett.* **2018**, *7* (10), 1208–1214.

(12) Goel, M.; Heinrich, C. D.; Krauss, G.; Thelakkat, M. Principles of Structural Design of Conjugated Polymers Showing Excellent Charge Transport toward Thermoelectrics and Bioelectronics Applications. *Macromol. Rapid Commun.* **2019**, 1800915.

(13) Lohwasser, R. H.; Thelakkat, M. Toward Perfect Control of End Groups and Polydispersity in Poly(3-Hexylthiophene) via Catalyst Transfer Polymerization. *Macromolecules* **2011**, *44* (9), 3388–3397.

(14) Iovu, M. C.; Sheina, E. E.; Gil, R. R.; McCullough, R. D. Experimental Evidence for the Quasi-"Living" Nature of the Grignard Metathesis Method for the Synthesis of Regioregular Poly(3-Alkylthiophenes). *Macromolecules* **2005**, *38* (21), 8649–8656.

(15) Yokoyama, A.; Miyakoshi, R.; Yokozawa, T. Chain-Growth Polymerization for Poly(3-Hexylthiophene) with a Defined Molecular Weight and a Low Polydispersity. *Macromolecules* **2004**, *37* (4), 1169–1171.

(16) Inal, S.; Malliaras, G. G.; Rivnay, J. Benchmarking Organic Mixed Conductors for Transistors. *Nature Communications* **2017**, *8* (1).

(17) Paulsen, B. D.; Tybrandt, K.; Stavrinidou, E.; Rivnay, J. Organic Mixed Ionic–Electronic Conductors. *Nat. Mater.* **2019**.

(18) Simon, D. T.; Gabrielsson, E. O.; Tybrandt, K.; Berggren, M. Organic Bioelectronics: Bridging the Signaling Gap between Biology and Technology. *Chemical Reviews* **2016**, *116* (21), 13009–13041.

(19) Rivnay, J.; Inal, S.; Salleo, A.; Owens, R. M.; Berggren, M.; Malliaras, G. G. Organic Electrochemical Transistors. *Nature Reviews Materials* **2018**, *3* (2), 17086.

(20) Cendra, C.; Giovannitti, A.; Savva, A.; Venkatraman, V.; McCulloch, I.; Salleo, A.; Inal, S.; Rivnay, J. Role of the Anion on the Transport and Structure of Organic Mixed Conductors. *Adv. Funct. Mater.* **2019**, *29* (5), 1807034.

(21) Savva, A.; Cendra, C.; Giugni, A.; Torre, B.; Surgailis, J.; Ohayon, D.; Giovannitti, A.; McCulloch, I.; Di Fabrizio, E.; Salleo, A.; Rivnay, J.; Inal, S. Influence of Water on the Performance of Organic Electrochemical Transistors. *Chemistry of Materials* **2019**, *31* (3), 927–937.

(22) Giovannitti, A.; Sbircea, D.-T.; Inal, S.; Nielsen, C. B.; Bandiello, E.; Hanifi, D. A.; Sessolo, M.; Malliaras, G. G.; McCulloch, I.; Rivnay, J. Controlling the Mode of Operation of Organic Transistors through Side-Chain Engineering. *Proceedings of the National Academy of Sciences* **2016**, *113* (43), 12017–12022.

(23) ElMahmoudy, M.; Inal, S.; Charrier, A.; Uguz, I.; Malliaras, G. G.; Sanaur, S. Tailoring the Electrochemical and Mechanical Properties of PEDOT:PSS Films for Bioelectronics. *Macromolecular Materials and Engineering* **2017**, *302* (5), 1600497.

(24) Flagg, L. Q.; Bischak, C. G.; Onorato, J. W.; Rashid, R. B.; Luscombe, C. K.; Ginger, D. S. Polymer Crystallinity Controls Water Uptake in Glycol Side-Chain Polymer Organic Electrochemical Transistors. *Journal of the American Chemical Society* **2019**, *141* (10), 4345–4354.

(25) Dong, B. X.; Nowak, C.; Onorato, J. W.; Strzalka, J.; Escobedo, F. A.; Luscombe, C. K.; Nealey, P. F.; Patel, S. N. Influence of Side-Chain Chemistry on Structure and Ionic Conduction Characteristics of Polythiophene Derivatives: A Computational and Experimental Study. *Chemistry of Materials* **2019**, *31* (4), 1418–1429.

(26) Wustoni, S.; Savva, A.; Sun, R.; Bihar, E.; Inal, S. Enzyme-Free Detection of Glucose with a Hybrid Conductive Gel Electrode. *Adv. Mater. Interfaces* **2019**, *6* (1), 1800928.

(27) Heinrich, C. D.; Thelakkat, M. Poly-(3-Hexylthiophene) Bottlebrush Copolymers with Tailored Side-Chain Lengths and High Charge Carrier Mobilities. *Journal of Materials Chemistry C* **2016**, *4* (23), 5370–5378.

(28) Balko, J.; Lohwasser, R. H.; Sommer, M.; Thelakkat, M.; Thurn-Albrecht, T. Determination of the Crystallinity of Semicrystalline Poly(3-Hexylthiophene) by Means of Wide-Angle X-Ray Scattering. *Macromolecules* **2013**, *46* (24), 9642–9651.

(29) Balko, J.; Portale, G.; Lohwasser, R. H.; Thelakkat, M.; Thurn-Albrecht, T. Surface Induced Orientation and Vertically Layered Morphology in Thin Films of Poly(3-Hexylthiophene) Crystallized from the Melt. *J. Mater. Res.* **2017**, *32* (10), 1957–1968.

(30) Mei, J.; Kim, D. H.; Ayzner, A. L.; Toney, M. F.; Bao, Z. Siloxane-Terminated Solubilizing Side Chains: Bringing Conjugated Polymer Backbones Closer and Boosting Hole Mobilities in Thin-Film Transistors. *J. Am. Chem. Soc.* **2011**, *133* (50), 20130–20133.

(31) Wustoni, S.; Combe, C.; Ohayon, D.; Akhtar, M. H.; McCulloch, I.; Inal, S. Membrane-Free Detection of Metal Cations with an Organic Electrochemical Transistor. *Adv. Funct. Mater.* **2019**, *29* (44), 1904403.

(32) Liu, F.; Chen, D.; Wang, C.; Luo, K.; Gu, W.; Briseno, A. L.; Hsu, J. W. P.; Russell, T. P. Molecular Weight Dependence of the Morphology in P3HT:PCBM Solar Cells. *ACS Appl. Mater. Interfaces* **2014**, *6* (22), 19876–19887.

(33) Proctor, C. M.; Rivnay, J.; Malliaras, G. G. Understanding Volumetric Capacitance in Conducting Polymers. *J. Polym. Sci. Part B: Polym. Phys.* **2016**, *54* (15), 1433–1436.

(34) Sivaraman, P.; Mishra, S. P.; Bhattacharrya, A. R.; Thakur, A.; Shashidhara, K.; Samui, A. B. Effect of Regioregularity on Specific Capacitance of Poly(3-Hexylthiophene). *Electrochimica Acta* **2012**, *69*, 134–138.

(35) Savva, A.; Wustoni, S.; Inal, S. Ionic-to-Electronic Coupling Efficiency in PEDOT:PSS Films Operated in Aqueous Electrolytes. *J. Mater. Chem. C* **2018**, *6* (44), 12023–12030.

(36) Rodahl, M.; Kasemo, B. A Simple Setup to Simultaneously Measure the Resonant Frequency and the Absolute Dissipation Factor of a Quartz Crystal Microbalance. *Review of Scientific Instruments* **1996**, *67* (9), 3238–3241.

(37) Rodahl, M.; Höök, F.; Krozer, A.; Brzezinski, P.; Kasemo, B. Quartz Crystal Microbalance Setup for Frequency and *Q* -factor Measurements in Gaseous and Liquid Environments. *Review of Scientific Instruments* **1995**, *66* (7), 3924–3930.

(38) Höök, F.; Rodahl, M.; Brzezinski, P.; Kasemo, B. Energy Dissipation Kinetics for Protein and Antibody–Antigen Adsorption under Shear Oscillation on a Quartz Crystal Microbalance. *Langmuir* **1998**, *14* (4), 729–734.

TOC GRAPHIC